Predicting color and short-circuit current of colored BIPV modules

Cite as: AIP Advances **11**, 095104 (2021); https://doi.org/10.1063/5.0063140
Submitted: 12 July 2021 • Accepted: 17 August 2021 • Published Online: 02 September 2021

T. Gewohn, C. Schinke, B. Lim, et al.

Predicting color and short-circuit current of colored BIPV modules

Cite as: AIP Advances 11, 095104 (2021); doi: 10.1063/5.0063140
Submitted: 12 July 2021 • Accepted: 17 August 2021 •
Published Online: 2 September 2021

T. Gewohn,[a),b)] C. Schinke,[b)] B. Lim, and R. Brendel[b)]

AFFILIATIONS

Institute for Solar Energy Research Hamelin (ISFH), Am Ohrberg 1, 31860 Emmerthal, Germany

[a)]**Author to whom correspondence should be addressed:** t.gewohn@isfh.de
[b)]**Also at:** Department Solar Energy, Leibniz University Hannover, Appelstr. 2, 30167 Hannover, Germany.

ABSTRACT

Photovoltaic modules for façade integration should have a widely modifiable appearance to adjust to the architect's requirements. However, architects today usually have only a limited number of already manufactured samples to choose from. Changing the color will also change the photovoltaic yield. Therefore, it would be helpful to have a procedure that allows us to determine the appearance and expected yield in advance of module fabrication. We present such a method for creating a digital prototype of a colored building integrated photovoltaic module. Using reflectance and external quantum efficiency measurements of eight colored modules, we simulate the appearance and respective energy yield for arbitrary module colors. We validate our predictions for 29 different colored modules. We use textiles that have been colored by printing and laminate them onto the modules to change the appearance of the modules. However, our digital prototyping model is also applicable to other coloring techniques. We achieve an average color difference of ΔE_{00} = 1.34 between predicted and measured colors, which is barely perceptible to the human eye. The predicted short-circuit current density of the digital prototype deviates on average less than 1% from the measured one.

I. INTRODUCTION

Due to climate and energy targets in the building sector, building integrated photovoltaics (BIPV) are developing from a niche product to an important market.[1] As a result of the lower costs for photovoltaic modules, the costs of standard BIPV modules are in the same price segment as non-PV façade and roof elements.[2] Numerous methods have been developed to alter the appearance of BIPV modules.[1] These techniques differ in terms of color impression, energy yield, and costs. The focus is often to hide the solar cells and to integrate the PV modules into the building envelope as unobtrusively as possible. Coloring the modules implies a reduction of the energy yield because a part of the incident light is reflected and is thus not used for energy generation.

This leads to two factors that push the cost of colored PV modules. First, the module price per surface area is increased because of the additional coloring process. Second, the reduced energy yield increases the cost of the generated electricity. Mass production of colored PV modules could address the first issue. However, mass production is apparently prevented by necessity for a highly individualized appearance of the modules required by architects.

For optimized planning at the beginning of the overall building process, it is therefore highly advantageous to offer to the architects any appearance that could be generated with a specific coloring technique before actually manufacturing the module and also to know the energy yield for any possible appearance.

How different colors affect the energy yield of solar cells and photovoltaic modules has already been discussed in theory.[2,3] Halme and Mäkinen[3] investigated the theoretical efficiency limits of ideal colored opaque photovoltaics. These authors did not consider a specific solar cell technology but an ideal single-bandgap solar cell. It was assumed that only a small fraction of the visible light is reflected for creating the respective color impression. The colors and the yield depend strongly on the relative luminosity. The relative luminosity can take any value between 0 and 1, where a perfectly white solar cell corresponds to 1 and an absolutely black one to 0. For example, at the theoretical limit, the energy loss for a bright white solar cell with a relative luminosity of 0.909 is 28% lower than the efficiency of an ideal black solar cell.

Peharz and Ulm calculated the power losses of crystalline silicon solar cells for the RAL colors that are commonly used and standardized in the industry.[2] For this purpose, they measured the

reflection spectra of RAL colors and calculated the color coordinates in the Commission Internationale de l'Éclairage (CIE)-XYZ color space. They recreated these color coordinates by combining two narrow reflective wavelength regions for c-Si solar cells. In contrast to the work of Halme and Mäkinen, the reflectance in this region was variable and not fixed at 100%, but the width of the reflective wavelength region was defined to be 20 and 40 nm, respectively. The resulting loss in short-circuit current density was determined using a two-diode model and is less than 20% for all RAL colors. However, the practical implementation of RAL colors by combining two small reflection ranges of 20–40 nm widths is difficult. Color pigments normally cause a much broader reflection spectrum. With such broader reflection spectra, Peharz *et al.* simulated the RAL colors with losses in the short-circuit current density of up to 90%. However, the measured RAL reflectance spectra also show high reflectance in the near-infrared region. This wavelength range does not contribute to the coloration but is responsible for energy losses.

In this work, we present a digital prototype of a PV module, i.e., a mathematical model for predicting the appearance and yield of an arbitrarily colored PV module whose appearance has been altered by laminating colored textiles (CoTex) onto the front glass of the module.[4] Applied colors, whether by CoTex, ceramic printing, or another coloring technique, always appear darker than without a PV module underneath due to the dark blue solar cells in the background. The digital prototype is used to determine the appearance of the finished PV module, i.e., the influence of the solar cells on the appearance is included. We simulate all achievable color variations and the resulting short-circuit current densities by using the reflection and external quantum efficiency (EQE) measurements of a set of eight colored PV modules only. We confirm the simulation results by experimental investigations. Note that the presented method is not limited to the CoTex technique but may be applied to other coloring techniques as well.

II. THEORY

In the theory section, we briefly present the basics of color vision and the principle of halftone printing. Both aspects are important for understanding the theory behind the equations we use for calculating the reflectance spectrum of a printed medium. We give a detailed derivation of the equations we use for calculating the reflectance spectrum of a printed medium in Appendix A.

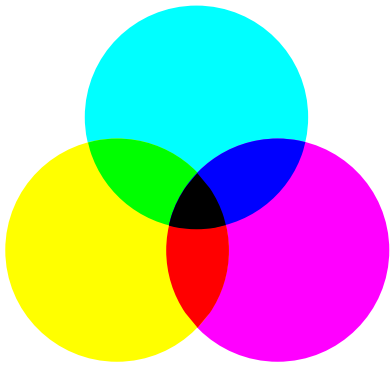

FIG. 1. Illustration of subtractive color mixing.

A. Color vision

The color of an object depends on its reflection spectrum. In the case of colored BIPV modules whose color impression is generated by a printed layer above the solar cell, the reflection spectrum is dominated by this colored layer and the solar cell below it. For an already manufactured PV module, only the reflection spectrum of the colored layer is variable. Printed colors are created by subtractive color mixing: Each printed ink absorbs a specific part of the incident spectrum, and the inks thus act as optical filters and change the reflection spectrum of the respective surface. Figure 1 shows the subtractive color mixing with the CMY system, which is used in this work. It contains cyan (C), magenta (M), and yellow (Y) as primary colors. If, for example, the color red is to be generated, magenta and yellow are mixed at a ratio of 1:1 so that only the wavelength range perceived as red by the human eye is being reflected. If a surface is covered by all three basic colors at 100% each, no light is reflected and the human eye perceives the color black. We use the CIE (Commission Internationale de l'Éclairage) XYZ color space to simulate the appearance of the module.[5] To calculate the X, Y, and Z values of the CIE XYZ color system, the three color-matching functions $\bar{x}$, $\bar{y}$, and $\bar{z}$, the reflection spectrum of the PV module and a relative spectral power distribution (SPD) are needed. The color matching functions are weighting functions for the light sensitivity of the three different cone cells of the eye of an average person. They are defined in the wavelength range from 360 to 830 nm. Figure 2 shows the color matching functions of the CIE 10° standard observer and the

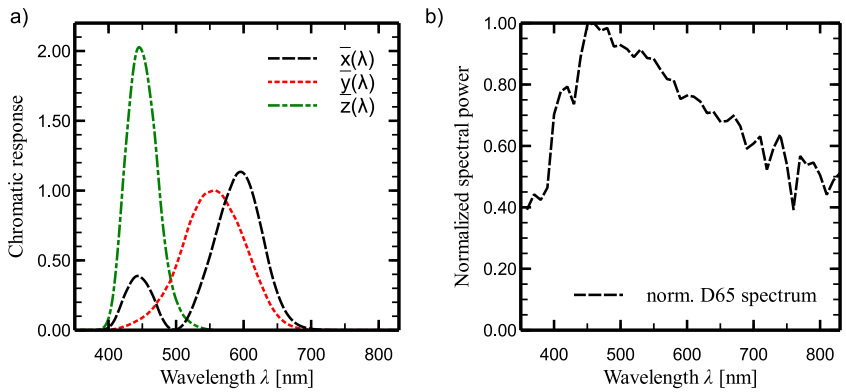

FIG. 2. (a) Color matching functions $\bar{x}$, $\bar{y}$, and $\bar{z}$ of the CIE color space. (b) CIE Standard Daylight Illuminant D65.

CIE Standard Daylight Illuminant D65 as the relative SPD, which we use for the simulations.[5] With the wavelength λ and the reflection spectrum $R(\lambda)$, we determine the X, Y, and Z values of the CIE color system using

$$X = \int_{360\ \mathrm{nm}}^{830\ \mathrm{nm}} R(\lambda)D65(\lambda)\bar{x}(\lambda)d\lambda,$$
$$Y = \int_{360\ \mathrm{nm}}^{830\ \mathrm{nm}} R(\lambda)D65(\lambda)\bar{y}(\lambda)d\lambda, \quad (1)$$
$$Z = \int_{360\ \mathrm{nm}}^{830\ \mathrm{nm}} R(\lambda)D65(\lambda)\bar{z}(\lambda)d\lambda.$$

In order to represent the three-dimensional color space more simply, the Z-component for each point of the color chart is determined mathematically from the other two by the relationship $x + y + z = 1$. When x and y are defined by

$$x = \frac{X}{X+Y+Z} \quad \text{and} \quad y = \frac{Y}{X+Y+Z}, \quad (2)$$

each X, Y, and Z of the triple can be associated with a color from the CIE chromaticity diagram that is shown in Fig. 3.

The color distance ΔE_{00}[6] quantifies the differences between any two colors. It is defined such that a ΔE_{00} value for any color is perceived by an average person as the same color difference. A color distance ΔE_{00} of any two colors that is smaller than 2 is only perceptible at close observation for the average person.[7] Figure 3(a) shows the chromaticity diagram in which four color distances ΔE_{00}, related to a specific color, are drawn as an example. Furthermore, for the second color, six significantly smaller color distances are drawn, and Fig. 3(b) shows an enlargement of these distances.

B. Halftone printing

The halftone printing technique creates a homogeneous color impression with three basic colors in a dot pattern.[8] The size and density of the dots vary depending on the print coverage and the required color impression. A mixed color is produced in halftone printing by a specific mixture of the three inks cyan (c), magenta (m), and yellow (y). The three ink screens are rotated relative to each other, typically at 30∘intervals, in order to avoid conspicuous periodic screens caused by the Moiré effect.[9] Figure 4 shows the rotation of the ink screens and the resulting color mixing. Depending on the selected printing parameters, there is an overlap of certain ink spots so that in addition to the unmixed inks, the mixed colors red (r), green (g), blue (b), and black (k) are created. Between these ink spots, there are also unprinted, i.e., white (w) areas. This results in eight different colored elements on the surface, which are called colorants.

Figure 5 shows (a) the optical microscopy image and (b) a camera shot of a sample printed with 50% magenta and 50% yellow, giving a terracotta-colored impression. In the microscopy image, individual dots and the rotation of the ink screens are visible.

C. Reflection spectrum of an imprinted object

For the simulation of the appearance of any mixed color, we use a modified version of the Clapper–Yule model.[10] This model was developed for the prediction of the reflection spectrum of halftone-printed colors on paper. It accounts for internal reflections and is based on reflection measurements of the eight colorants. We use this model to determine the reflectance R_{print} of a printed PV module based on which we can simulate the color of the module.

We determine the surface coverage a_j of the inks used using Demichel's equations[11] as follows:

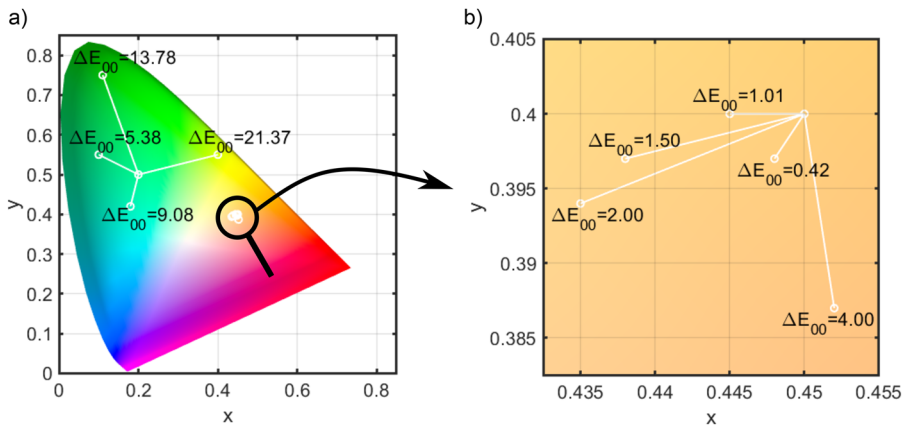

FIG. 3. CIE chromaticity diagram, created using MATLAB. For two colors ($x_1 = 0.2, y_1 = 0.5$ and $x_2 = 0.45$, $y_2 = 0.4$), we give the distance ΔE_{00} to four and six, respectively, related to other colors. The respective colors are marked by a white circle, and the color pairs are connected by a line. (a) The entire chromaticity diagram and (b) an enlargement of the area with the plotted colors and the respective ΔE_{00} values.

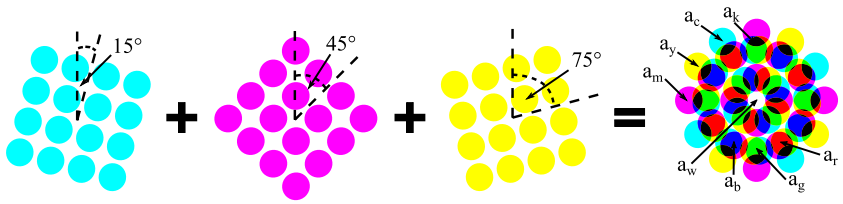

FIG. 4. In halftone printing, the inks are rotated in relation to each other. The colors a_c, a_m, a_y, a_r, a_g, a_b, a_k, and a_w, which result from the overlaying of printed inks, are called colorants.

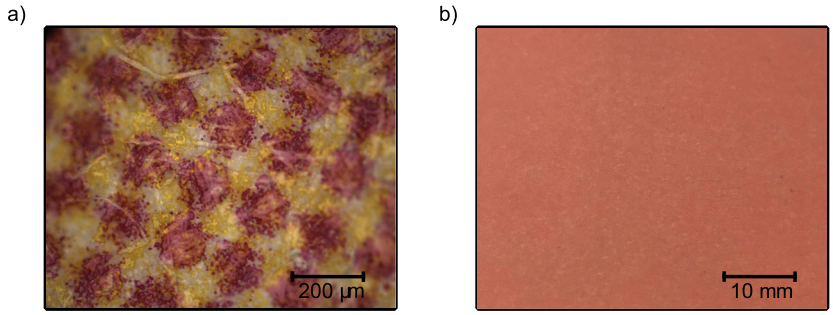

FIG. 5. Image obtained with (a) an optical microscope and (b) a digital camera of a sample printed with 50% magenta and 50% yellow.

$$\begin{aligned} a_w &= (1-c)(1-m)(1-y), & a_c &= c(1-m)(1-y), \\ a_m &= (1-c)m(1-y), & a_y &= (1-c)(1-m)y, \\ a_r &= (1-c)my & a_g &= c(1-m)y, \\ a_b &= \mathrm{cm}(1-y), & a_k &= cmy, \end{aligned} \tag{3}$$

and we calculate R_{print} using the Clapper–Yule model as follows:[12]

$$R_{print}(\lambda) = r_{spec} + \frac{(1-r_{spec})r_g(\lambda)\left[\sum_{j=1}^{8} a_j t_j(\lambda)\right]^2 (1-r_{int})}{1 - r_{int} r_g(\lambda)\left[\sum_{j=1}^{8} a_j t_j^2(\lambda)\right]}. \tag{4}$$

The specular r_{spec} and the internal reflection r_{int} can be calculated numerically via the Fresnel equations.[13] For the determination of the transmission $t_j(\lambda)$ through colorant j, only the reflectance $R_j(\lambda)$ of the material printed with colorant j must be measured. Using the measured reflection spectrum R_w of the unprinted medium, the Lambertian reflection $r_g(\lambda)$ is

$$r_g(\lambda) = \frac{R_w(\lambda)}{(1-r_{int})(1-r_{spec}) + R_w(\lambda) r_{int}}, \tag{5}$$

and the transmission of the certain colorants can be calculated using

$$t_j(\lambda) = \sqrt{\frac{R_j(\lambda) - r_{spec}}{r_g(\lambda)[(R_j(\lambda) r_{int} + (1-r_{int})(1-r_{spec})]}}. \tag{6}$$

We provide a detailed derivation of the equations we use in Appendix A.

III. EXPERIMENTAL METHODS

A. Sample preparation

1. Fabrication of the customized PV modules

Figure 6 shows the structure of the CoTex BIPV modules.[14] It is composed of a commercially available PV module and a laminated additional layer system on top.

We prepare a one-cell PV module using a 156 × 156 mm^2 silicon solar cell with silver fingers on the front and a full-area aluminum metallization on the rear. The cell is contacted on the front and the rear with the smart wire technology.[15] The module has a three-film transparent backsheet (FPL-FET-T250-T50, Toyal Solar) on the bottom. The cell is encapsulated with UV-transmissive EVA (EVASKY S87, Bridgestone) with a thickness of 460 μm and has a low-iron glass plate with a thickness of 4 mm on the top. The CoTex layer system consists of a nonwoven fabric (Freudenberg Performance Light Diffuser with 50 g/m^2, FPLD50, Freudenberg Performance Materials[16]) embedded between the two layers of the UV-absorbing polyolefin encapsulant (Solar Encapsulant Film PO8510, 3M) and is covered with a transparent front sheet (FPL-FET-T250-T50, Toyal Solar). We use the refractive index matching liquid paraffin to temporarily couple the CoTex layer system optically to the PV module in the experiments reported here. This facilitates the screening of a large number of different CoTex layers using the same PV module. Köntges *et al.* demonstrated that this method yields the same results as a permanent lamination.[17] The "Freudenberg Performance Light Diffuser" used in this work is a nonwoven fabric for LED lighting systems. It consists of polyester fibers and combines high transmission and strong light diffusion. Note that a wide range of other textile materials may also be used.[14]

2. Coloring of the nonwoven fabrics

We print on the textiles with the offset print technique and in halftone. Figure 7 shows 37 different colors that we print on an area of 5 × 5 cm^2 each on FPLD50. The colors are different combinations of the inks cyan, magenta, and yellow with the respective print coverages of 0%, 25%, 50%, 75%, and 100%. The eight colors in row A correspond to the eight colorants introduced in Sec. II B (see Fig. 4) and provide the basis for the simulation. The other 29 color variations are used for the experimental validation of the simulation.

Figure 8 shows a photograph of the corresponding 37 differently printed CoTex layers. Note that for this photograph, the samples were optically coupled with paraffin to a PV module consisting of 30 half cells and a total size of 850 × 520 mm^2. Through this, we get an overview of all 37 samples under the same lighting and background conditions. As described above, all reflectance and EQE measurements are performed by coupling to a one-cell module.

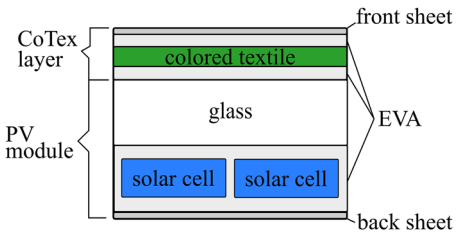

FIG. 6. Schematic of the CoTex PV modules.

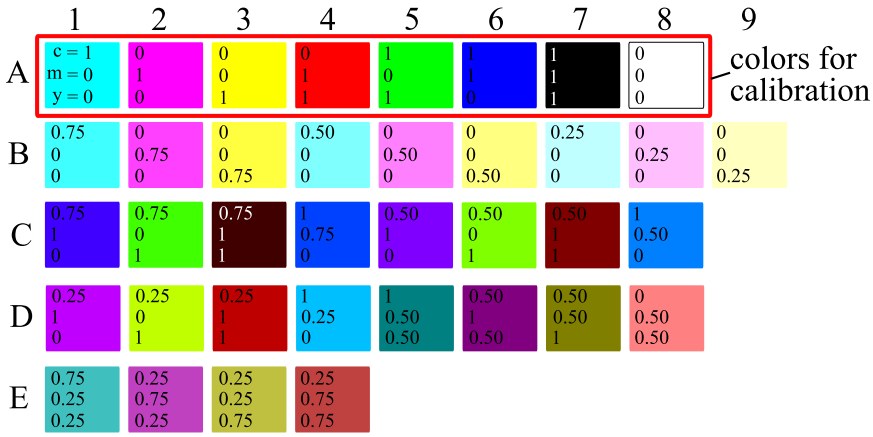

FIG. 7. Print pattern for the calibration and the validation of the simulation. The print coverages for cyan (c), magenta (m), and yellow (y) are given in the fields.

B. Measurements

1. Reflection measurements

We measure the reflection spectrum of all samples in a wavelength range from 360 to 830 nm in 1 nm steps using a photospectrometer (Cary 5000, Agilent Technologies, CA, USA) with an integrating sphere of 15 cm in diameter. The illumination angle is 7 to the normal of the sample, and the illuminating spot has a radius of 18 mm.

2. EQE measurements

We perform spectrally resolved external quantum efficiency (EQE) measurements in a wavelength range from 300 to 1200 nm using the LOANA system (PV-Tools GmbH, Hamelin, Germany). The illumination direction is perpendicular to the sample, and the illuminated spot is 20×20 mm^2. The LOANA system uses a bias background illumination to measure the solar cell at the working level of 300 W/m^2 and thus follows the IEC 60904-8 standard.[18]

C. Simulation of the color

1. Simulation of the reflection spectrum

We use Eqs. (5) and (6) and the measured reflection spectra of the eight samples where only one colorant is present (row A in Fig. 7) to calculate the parameters $t_j(\lambda)$ and $r_g(\lambda)$. Assuming an index of refraction of $n = 1.5$ for the imprinted layer and $n = 1$ for air, the Fresnel formulas give the constant values $r_{int} = 0.596$ and $r_{spec} = 0.04$.[13] Using Eq. (3), we calculate the surface coverages a_j and simulate the reflection spectra $R_{CoTex}(\lambda)$ of the 29 other color variations. Knowing $R_{CoTex}(\lambda)$, we can determine the x- and y-coordinates in the color space using Eqs. (1) and (2). In Appendix B, Fig. 19(a) shows the Lambertian reflectance $r_g(\lambda)$ calculated using Eq. (5) and the transmission calculated using Eq. (6) for the colorants cyan, magenta, and yellow as an example.

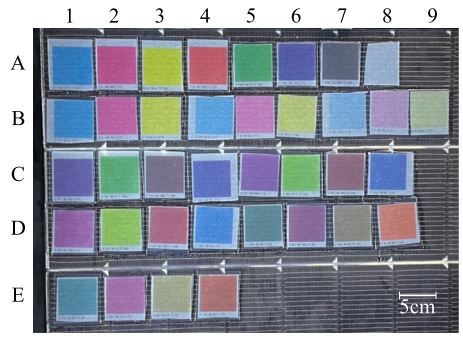

FIG. 8. Photograph of prepared samples in different colors (as shown in Fig. 7) for the calibration and validation of the simulation.

2. Prediction accuracy

We evaluate the consistency between the simulated and measured colors with the CIELAB ΔE_{00} criterion (see Sec. II A and Ref. 6). The ΔE_{00} criterion is a quantitative measure for the perceived color distance. For details on the calculation of ΔE_{00}, we refer to Ref. 19.

D. Simulation of the energy yield

The wavelength-dependent external quantum efficiency (EQE) of a photovoltaic module is a measure of how many of the incident photons are converted to charge carriers that are collected at the contacts and therefore contribute to the generated electric current. In combination with the open-circuit voltage and the fill factor, the short-circuit current density (J_{SC}) determines the energy yield of a photovoltaic module. We have shown in Ref. 4 that by altering the appearance using CoTex layers, the J_{SC} value in particular is reduced. For simplification, we thus assume that the module output power and J_{SC} are proportional, i.e., the open-circuit voltage and fill factor do not change due to the application of CoTex layers. When we specify the energy yield of a CoTex BIPV module, we always follow this simplification and refer to the measured or simulated J_{SC} value.

We calculate J_{SC} for any given color, i.e., any possible combination of the inks cyan, magenta, and yellow, from the simulated EQE as described in Sec. III D 1.

1. Simulation of the external quantum efficiency

For the simulation of the EQE of any given color, we use the same procedure as for the simulation of the reflection spectra.

Instead of the reflection, we now consider the relative transmission T_j as follows:

$$T_j(\lambda) = \frac{EQE_j(\lambda)}{EQE_{ref}}, \tag{7}$$

where $EQE_j(\lambda)$ is the measured EQE of colorant j and EQE_{ref} is the measured EQE of the one-cell module without a CoTex layer. Replacing the reflections of the individual colorants in Eq. (4) by the transmissions of the colorants yields the transmission of a CoTex layer as follows:

$$\begin{aligned} t_g(\lambda) &= \frac{T_w(\lambda)}{(1-r_{int})(1-r_{spec}) + T_w(\lambda) r_{int}}, \\ t_j(\lambda) &= \sqrt{\frac{T_j(\lambda) - r_{spec}}{t_g(\lambda)[(T_j(\lambda) r_{int} + (1-r_{int})(1-r_{spec})]}}, \\ T_{CoTex}(\lambda) &= \frac{(1-r_{spec}) t_g(\lambda) \left[\sum_{j=1}^{2^k} a_j t_j(\lambda)\right]^2 (1-r_{int})}{1 - r_{int} t_g(\lambda) \left[\sum_{j=1}^{2^k} a_j t_j^2(\lambda)\right]}. \end{aligned} \tag{8}$$

All other variables and indices are identical to the simulation of the reflection in Eqs. (3) and (4). In contrast to the simulations of the reflectance, where only the wavelength range from 360 to 830 nm is investigated, we consider wavelengths from 300 to 1200 nm for the measured and the simulated EQE. Multiplying the simulated transmission of the CoTex layer by EQE_{ref} gives the EQE of the CoTex module: $EQE_{CoTex} = T_{CoTex}(\lambda) \cdot EQE_{ref}(\lambda)$. In Appendix B, Fig. 19(b) shows as an example the relative transmissions $T_c(\lambda)$, $T_m(\lambda)$, and $T_y(\lambda)$ of samples A1, A2, and A3 calculated using Eq. (7) and the internal transmission $t_g(\lambda)$ determined using Eq. (8).

2. Calculation of the short-circuit current density

We calculate the short-circuit current density using

$$J_{SC} = q \int_{300\,\text{nm}}^{1200\,\text{nm}} d\lambda \Phi_0(\lambda) EQE(\lambda), \tag{9}$$

with the module's EQE, the elementary charge q, and the wavelength λ-dependent AM1.5G photon flux $\Phi_0(\lambda)$.[20,21]

E. Consequences of printing inaccuracies

The simulations presented provide the expected appearance of a CoTex module and its energy yield for specific printing parameters, i.e., the inks cyan, magenta, and yellow in certain print coverages. Since printers have an uncertainty when printing, we simulate the effect on appearance and yield if an ink is printed with 3% more or less print coverage than intended. We consider all combinations of the three inks in print coverage between 0% and 100% in 10% steps, resulting in 1331 colors. For each of the 1331 colors, the coverage of one, two, and all three inks is successively first reduced and then increased by 3% compared to the intended value, resulting in 26 variations of each color. The variations consist of all possible combinations of the (0.97, 1, 1.03) triple for each of the three primary colors cyan, magenta, and yellow. That is, we assess the impact if the respective ink is being printed with 97%, 100%, or 103% of the planned print coverage. The effect of the printing inaccuracy is determined by considering the color difference ΔE_{00} and the difference in short-circuit current density to the original color.

IV. RESULTS

A. Simulation accuracy

1. Accuracy of the simulation of the appearance

Using the measured reflection spectra of the CoTex modules in the eight colors in row A (Fig. 7) and Eqs. (3) and (4), we simulate the reflection spectra of the 29 samples in rows B to E and calculate the color coordinates according to Eqs. (1) and (2). We also calculate the color coordinates using the measured reflection spectra of the 29 samples. Figure 9 shows the color differences ΔE_{00} between the measured and simulated colors. The average ΔE_{00} value of all 29 values is 1.34.

Figure 10 shows the measured (blue triangles) and simulated (green squares) reflection spectra of the colors with (a) the lowest, (b) a moderate, and (c) the highest ΔE_{00} value. The background color of the area below the measured reflection spectrum represents the measured color, and the background color of the area above the simulated reflection spectrum represents the corresponding simulated color. In Fig. 10(a), with $\Delta E_{00,E4} = 0.46$, the reflection spectra of color D4 (C: 1, M: 0.25, and Y: 0) lie exactly on top of each other, and no difference between the two colors is perceptible. In Fig. 10(b), with $\Delta E_{00,B5} = 1.21$, the two reflection spectra deviate by up to 0.0074 in the wavelength range from 500 to 600 nm. However, no difference can be perceived between the measured and simulated colors. Figure 10(c) shows the largest difference between the measurement and simulation with $\Delta E_{00,D5} = 2.86$. The simulated reflection spectrum in the range between 400 and 500 nm is up to 0.016 higher than the measured reflection spectrum. Despite the differences in the reflection spectra, the perceivable color difference is very small. The simulated color appears slightly brighter than the measured one.

2. Accuracy of the simulation of J_{SC}

Using the measured EQE of the eight CoTex modules in row A of Fig. 7 and Eqs. (3) and (7)–(9), the EQE of the other 29 samples was simulated and J_{SC} was calculated, respectively. We compare

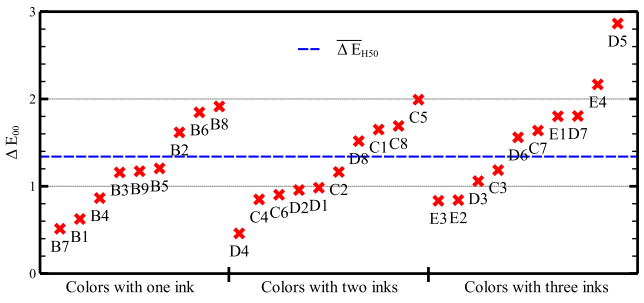

FIG. 9. Color distance ΔE_{00} between the colors calculated from measured and simulated reflectance spectra using Eqs. (1) and (2). The labels of the colors refer to the colors in Fig. 7. The blue dashed line shows the average value of $\Delta E_{00} = 1.34$.

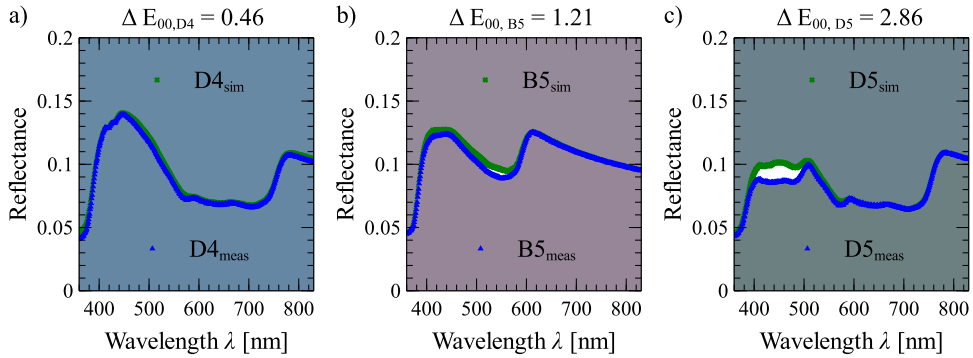

FIG. 10. Measured and simulated reflection spectra of samples with the (a) lowest ΔE_{00} (color D4), (b) a moderate ΔE_{00} (color B5), and (c) the highest ΔE_{00} (color D5) value. The background above and below the respective curve is colored in the color determined from the reflection spectrum. This illustrates the difference between the measured and simulated colors.

the results with J_{SC} calculated from the measured EQE of the 29 samples. The average ratio $r = \frac{J_{SC,\,simulated}}{J_{SC,\,measured}}$ of all simulated colors is 1.003. Figure 11 shows the deviation $\Delta r = |1 - r|$ of each sample. Δr is 0.008 on average.

In Fig. 12, differences in certain wavelength ranges become apparent when comparing measured (blue triangles) and simulated (green crosses) EQEs. Figure 12(a) shows the EQE of sample D7 (C: 0.5, M: 0.5, and Y: 1), the color with the smallest deviation between the measurement and simulation. Both curves are almost identical, and the maximum deviation is 0.03. With $\Delta r_{C5} = 0.008$, the deviation of color C5 (C: 0.5, M: 1, and Y: 0) in Fig. 12(b) is on average. Here, the simulated EQE in the range between 400 and 600 nm is lower than the measured EQE with a maximum deviation of 0.032 and higher in the range of 600–800 nm by up to 0.015. Figure 12(c) shows the EQE of color E4 (C: 0.25, M: 0.75, and Y: 0.75), with $\Delta r_{E4} = 0.009$ the highest deviation between simulation and measurement. The EQE is overestimated by up to 0.08 in the range between 400 and 750 nm. Remarkably, the inks have an influence on the visible wavelength range only. From 780 to 1200 nm, the EQE is identical for all colors. This fact is illustrated by the comparison with the measured EQE of sample A8 (red diamonds). Sample A8 is not imprinted. From a wavelength of ~800 nm, the EQEs of the printed samples and those of the unprinted sample overlap exactly.

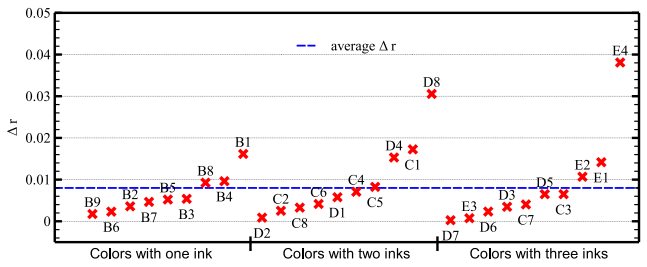

FIG. 11. Deviation Δr of the J_{SC}-ratios r calculated from the measured and simulated EQEs of the respective colored samples. The labels of the colors refer to the colors in Fig. 7. The blue dashed line shows the average value of $\Delta r = 0.008$.

3. Consequences of printing inaccuracies

We investigate the deviations from planned appearance and J_{SC} due to printing inaccuracies for 1331 different colors, as described in Sec. III E.

Figure 13(a) shows the ΔE_{00} value of all 26 variations for all 1331 colors in comparison to the planned color. For all printing accuracy variations and colors, ΔE_{00} is less than 1. The mean value is less than 0.5 for all variations. The highest mean value of $\Delta E_{00} = 0.47$ occurs in variation 20 with the triple (1.03, 0.97, 1.03). This means that cyan is printed with 103%, magenta with 97%, and yellow with 103% of the planned print coverage. With ΔE_{00} values below 1, the difference between the requested and the printed color is not perceptible, even in the worst case. Printer inaccuracies of up to 3% therefore have no noticeable impact on the color of the finished product.

Figure 13(b) shows the ratio between the J_{SC} value of the 26 variations and the J_{SC} value of the planned color. The mean value of the deviation is 0.006 in the worst case, and the mean deviation over all colors and variations is only 0.003. Thus, the difference that can occur due to inaccuracies in the printing process is marginal.

B. Combination of appearance and J_{SC}

Using the simulation method described above, we are able to simulate the appearance and short-circuit current density for all possible combinations of the three inks cyan, magenta, and yellow printed on a nonwoven fabric and attached to the one-cell module. Figure 14 shows the colors and the corresponding J_{SC} value of 125 simulations. All possible combinations of cyan, magenta, and yellow in the print coverages of 0%, 25%, 50%, 75%, and 100% were selected. We plot the relative short-circuit current density $J_{SC,\,rel.} = \frac{J_{SC,\ CoTex\ color}}{J_{SC,\ reference}}$, with $J_{SC,reference} = 33.93$ mA/cm^2 of the one-cell module without a CoTex layer.

In order to get a better overview of which colors are possible with which textile and which inks, we refer to the RAL 840-HR classic colors (RAL gGmbH, Bonn, Germany). These are standardized colors for the industry. Figure 15 illustrates the RAL colors of PV modules that we can produce with the CoTex layers of printed FPLD50. The corresponding $J_{SC,rel.}$ value shows that depending on

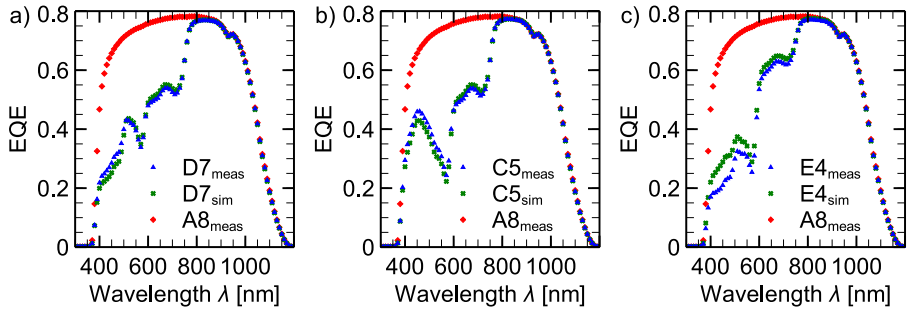

FIG. 12. Measured (blue triangles) and simulated (green crosses) EQEs of samples imprinted with colors (a) D7, (b) C5, and (c) E4. For comparison, the measured EQE of sample A8 and thus of the unprinted sample is also shown (red diamonds).

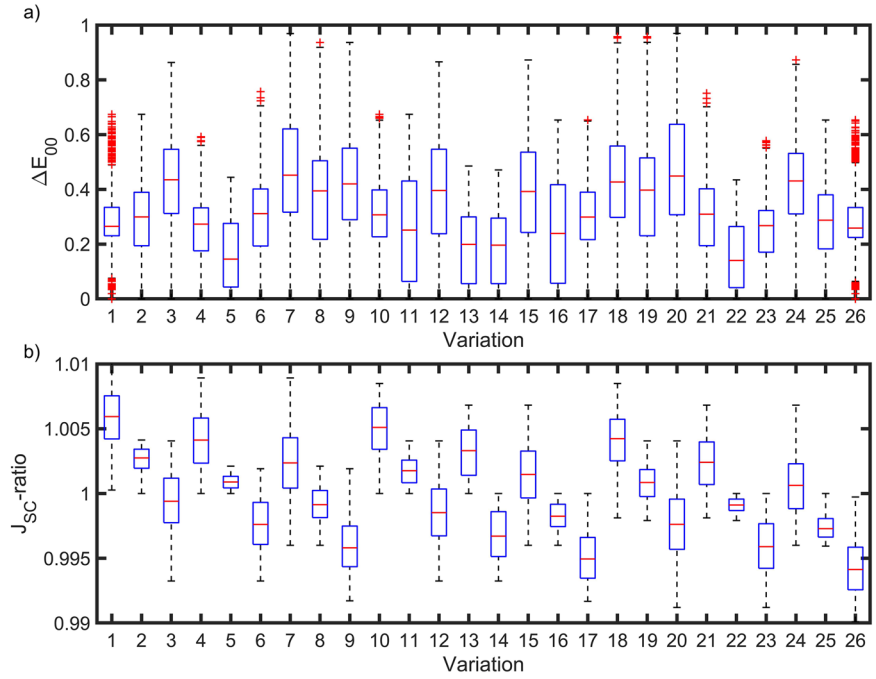

FIG. 13. (a) ΔE_{00} and (b) J_{SC} ratio of 26 potential deviations with a printing inaccuracy per ink of maximum 3% compared to the print with the exact printing parameters. This comparison was done for 1331 different colors.

the color selected, a J_{SC} value and thus an energy yield between 67% and 89% can be achieved compared to a PV module without a CoTex layer. The highest yield is achieved with the RAL 7040 color, which results when using unprinted FPLD50.

V. DISCUSSION—SIMULATION ACCURACY

With an average ΔE_{00} value of 1.34, the difference between the simulated and measured colors investigated in this work is hardly

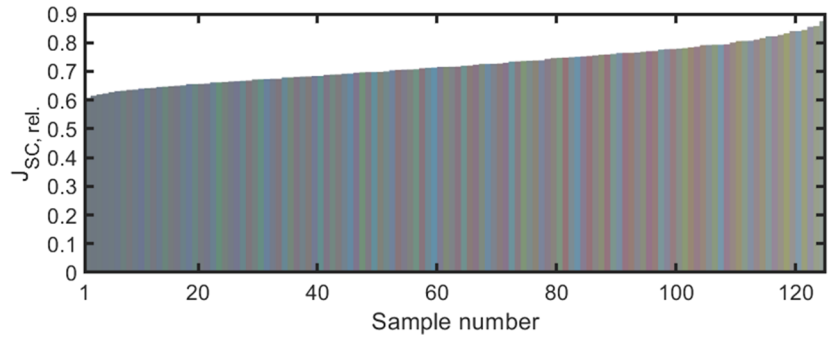

FIG. 14. Simulated colors with the respective $J_{SC,CoTex\ color}$ value relative to the $J_{SC,reference}$ value of the one-cell module without a CoTex layer.

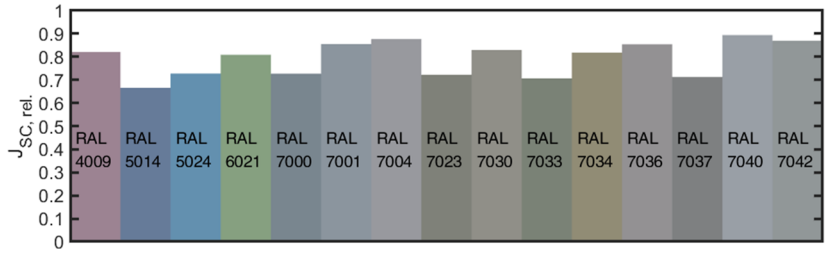

FIG. 15. Simulated RAL colors and the corresponding short-circuit current densities of CoTex modules that can be produced with the textile and inks used in this work.

noticeable. Note that we also evaluated other models for the simulation of the reflection spectrum, such as the cellular Yule–Nielsen model,[12] on a smaller sample size and found that the simulation accuracy is higher than for the model presented in this work. However, the cellular Yule–Nielsen model uses 27 colors for the calibration, whereas the model of Clapper and Yule requires only eight colors. By needing only eight samples for calibration, the advantage of cost and time savings outweighs in practice.

So far, our simulations use the one-cell module as a background. That is, we determine a single reflection spectrum of the photovoltaic module and neglect the metallization of the solar cell. In particular, busbars are not included and are not simulated. In our experience, it is indeed more difficult to achieve a homogeneous appearance when busbars are present. However, we did already demonstrate that the metallization is completely hidden by many textiles and colors and can usually only be seen up from a close distance. A detailed analysis of the masking of the solar cells at different textile densities, colors, and print coverages was done in Ref. 4. If PV modules with a black backsheet are used, there is sufficient homogeneity under the CoTex layer so that the PV modules appear homogeneous in one color. When using PV modules with white backsheets, the contrast with the solar cells is very high and the gaps between the cells are visible. In this case, the simulation of the appearance of the gaps between the cells should be performed. This allows us, on the one hand, to estimate how homogeneous the color impression will be. On the other hand, the planned print pattern can also be adjusted and thus compensate the inhomogeneities that arise.

VI. CONCLUSION

With the CoTex method, the ability to accurately predict the appearance of the finished module is particularly important because there is a huge difference between the appearance of the printed textile and the manufactured CoTex module. By encapsulating the printed textile, the appearance is already greatly changed. If this encapsulated textile is laminated onto a PV module, the color impression is altered even more due to the dark background. The simulation of the expected J_{SC} value is also essential since it is decisive for the payback time. In addition to these necessary points, the simulations offer several additional advantages.

The simulations can be used to precisely simulate which colors are possible with which textiles and with which energy yield. If multiple materials are investigated and available for selection, the simulation of the digital prototype can be used to find the optimal material for a desired color in order to achieve the highest possible energy yield.

The simulation of a digital prototype is also useful for other techniques to modify the appearance of PV modules. Even when using ceramic printing directly on the front glass, when using colored foils or colored glass, the appearance of the colored material differs from the color resulting in combination with the underlying solar cells. Furthermore, the energy yield is unknown without a fabricated sample or simulation when using a new color.

For a high acceptance, BIPV modules must be individually designable. Many techniques for coloring PV modules offer this individuality. Usually, sample modules have to be produced to see how it looks like and which power yield this module can generate. With the simulation of a digital prototype, we are able to determine the appearance and yield of a wide range of colored PV modules after manufacturing only a handful of calibration samples.

With our chosen model, only eight colored samples need to be produced and measured for the calibration of the simulation. Then, the appearance and short-circuit current density of any combination of different print coverages of the inks used can be simulated.

We determined the simulation accuracy using 29 different colored samples. The average color difference between the measured and simulated colors is $\Delta E_{00} = 1.34$, and for the simulated short-circuit current density, the deviation is $\Delta r = 0.008$ on average.

In this work, we chose the material FPLD50 for the CoTex method. With the combination of this textile and the used inks, we produced colored PV modules with a relative J_{SC} value between 60% and 89% in comparison to the reference PV module. Our proposed simulation of a digital prototype allows a simple and fast evaluation of other materials and paves the way to easily find the best combination of textiles, inks, and print coverages for each color to achieve the highest energy yield.

ACKNOWLEDGMENTS

This work was funded by the state of Lower Saxony. The publication of this article was funded by the Open Access Fund of Leibniz Universität Hannover.

APPENDIX A: DERIVATION OF THE CLAPPER-YULE MODEL

In the following, we derive the Clapper–Yule[10] model that we use to calculate the reflection spectrum of a PV module covered with a textile, imprinted with three inks in any combination of print thicknesses. We refer to the explanations of Hersch and Hébert.[12]

Figure 16 illustrates the modified model. The term T_{in} describes the losses of the incident light beam during the transition from air to the medium and the propagation through the colored layer. R_{int}

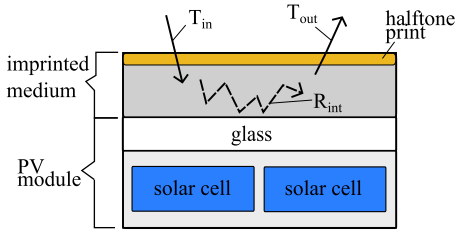

FIG. 16. Overview scheme showing the factors T_{in}, R_{int}, and T_{out} for calculating the reflectance R_{print} of a printed medium using the model of Clapper and Yule.

represents the reflections inside the medium. T_{out} describes the portion of the radiation that leaves the medium. Using these three terms, R_{print} is obtained using the following equation:

$$R_{print}(\lambda) = T_{in}(\lambda)R_{int}(\lambda)T_{out}(\lambda). \tag{A1}$$

To allow a better understanding, we will derive the three terms separately in detail in the following and merge them at the end.

a. First, we focus on the light T_{in} entering the medium. Figure 17(a) shows an incoming light beam at different locations on the surface of a medium, which is imprinted with cyan and magenta, both with a print coverage of 50%. At the interface between air and the sample, the reflectance is r_{spec}. The transmission through the colorant j depends on the surface coverage a_j and the wavelength λ dependent transmission $t_j(\lambda)$. In combination with the surface reflectance, this results in an attenuation of an incident light beam by a factor of $(1 - r_{spec})a_j t_j(\lambda)$.

Figure 17(b) shows the printed medium in the top view. The probability P_c for a light ray to hit the cyan-colored area a_c is the print coverage of cyan multiplied by the proportion of the area that is not magenta: $P_c = c \cdot (1 - m)$. Equivalently, the probabilities P_m, P_b, and P_w are determined as follows:

$$P_m = m \cdot (1 - c), \quad P_b = c \cdot m, \quad P_w = (1 - c)(1 - m), \tag{A2}$$

where the indices represent the respective colorant.

The probability for a light ray to hit a certain colorant thus defines the surface coverage of this colorant, which is $a_j = P_j$. When working with three inks, the proportions of the surface with the respective colorant can be determined using Demichel's equations as follows:[11]

$$\begin{aligned} a_w &= (1-c)(1-m)(1-y), & a_c &= c(1-m)(1-y), \\ a_m &= (1-c)m(1-y), & a_y &= (1-c)(1-m)y, \\ a_r &= (1-c)my, & a_g &= c(1-m)y, \\ a_b &= \mathrm{cm}(1-y), & a_k &= cmy. \end{aligned} \tag{A3}$$

Based on Fig. 17 and Eq. (A3), it follows with the incoming irradiation $E_0(\lambda)$

$$T_{in}(\lambda) = (1 - r_{spec}) \sum_{j=1}^{8} a_j t_j(\lambda) \cdot E_0(\lambda). \tag{A4}$$

b. The next aspect we consider is the internal reflection R_{int} as shown in Fig. 18(a). For paper and similar materials, we assume that incoming light T_{in} is affected by Lambertian scattering $r_g(\lambda)$, which depends on the material parameters. Thereby, T_{in} is diffusely scattered into the hemisphere in equal parts, leading to the angle-independent radiance

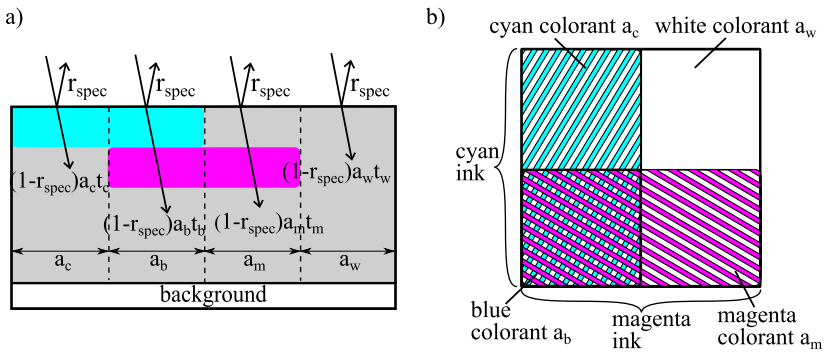

FIG. 17. Scheme of incoming light rays into the printed medium (a) and the top view of the printed medium (b). Illustration is based on Ref. 12.

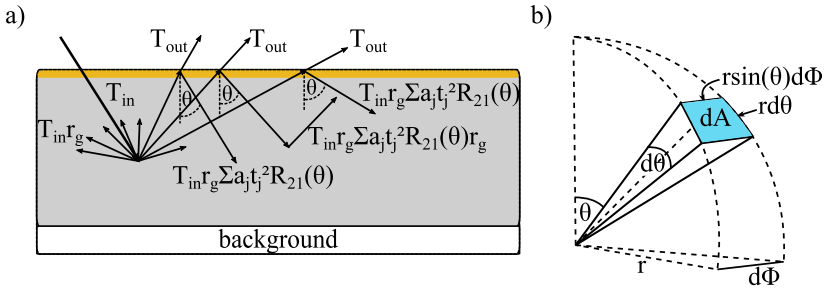

FIG. 18. (a) Incident radiation T_{in} is reflected in the substrate by Lambertian reflection r_g and Fresnel reflection $R_{21}(\theta)$. (b) The radiation is reflected equally distributed on the area element dA in the hemisphere. Illustration is based on Ref. 12.

$L = \frac{T_{in}(\lambda) r_g(\lambda)}{\pi}$. Figure 18(b) shows the radiation reaching an area element dA of the hemisphere with radius r. With the solid angle $d\Omega = \frac{dA}{r^2} = \sin\theta d\theta d\phi$, it follows for the irradiance $dE(\lambda) = \frac{T_{in}(\lambda) r_g(\lambda)}{\pi} \cos\theta d\Omega = \frac{T_{in}(\lambda) r_g}{\pi} \cos\theta \sin\theta d\theta d\phi$. When a light ray hits the interface between the printed layer and air, Fresnel reflection occurs. Part of the light is reflected back into the medium with the angle θ dependent reflection $R_{21}(\theta)$, and the other part, given by T_{out}, leaves the substrate. The reflected radiation is obtained by integration over the hemisphere as follows:

$$\begin{aligned} E_{reflected}(\lambda) &= \int_0^{2\pi} \int_0^{\pi/2} \frac{T_{in}(\lambda) r_g(\lambda)}{\pi} R_{21}(\theta) \cos\theta \\ &\quad \times \sin\theta d\theta d\phi \\ &= T_{in}(\lambda) r_g(\lambda) \int_0^{\pi/2} R_{21}(\theta) \sin 2\theta d\theta \\ &= T_{in}(\lambda) r_g(\lambda) r_{int}, \end{aligned} \tag{A5}$$

where r_{int} represents the angle- and wavelength-independent reflection at the boundary layer to air. If we also take into account the halftone layer, the radiation $E_1(\lambda)$ after one reflection cycle results in

$$E_1(\lambda) = T_{in}(\lambda) r_g(\lambda) \sum_{j=1}^{8} \left(a_j t_j(\lambda)^2\right) r_{int} r_g(\lambda). \tag{A6}$$

The consideration of infinite reflection cycles leads to the radiation $E_R(\lambda)$ reflected from the printed medium as follows:

$$\begin{aligned} E_R(\lambda) &= T_{in}(\lambda) r_g(\lambda) \sum_{k=1}^{\infty} \left[\sum_{j=1}^{8} \left(a_j t_j(\lambda)^2\right) r_{int} r_g(\lambda) \right]^k \\ &= \frac{T_{in}(\lambda) r_g(\lambda)}{1 - r_g(\lambda) r_{int} \sum_{j=1}^{8} a_j t_j(\lambda)^2}. \end{aligned} \tag{A7}$$

Thus, it follows for the factor of internal reflections

$$R_{\text{int}}(\lambda) = \frac{r_g(\lambda)}{1 - r_g(\lambda) r_{int} \sum_{j=1}^{8} a_j t_j(\lambda)^2}. \tag{A8}$$

c. The factor T_{out} describes the portion of the radiation that leaves the substrate as follows:

$$T_{out}(\lambda) = (1 - r_{int}) \sum_{j=1}^{8} a_j t_j(\lambda). \tag{A9}$$

1. Computation of the reflectance R_{print} of the imprinted medium

Using Eqs. (A4), (A9), and (A10), we obtain the total reflectance of the printed substrate as follows:

$$\begin{aligned} R_{print}(\lambda) &= T_{in}(\lambda) R_{int}(\lambda) T_{out}(\lambda) \\ &= r_{spec} + \frac{(1 - r_{spec}) r_g(\lambda) \left[\sum_{j=1}^{8} a_j t_j(\lambda)\right]^2 (1 - r_{int})}{1 - r_{int} r_g(\lambda) \left[\sum_{j=1}^{8} a_j t_j^2(\lambda)\right]}. \end{aligned} \tag{A10}$$

The two reflections r_{spec} and r_{int} can be calculated numerically via the Fresnel equations.[13] For the determination of the parameters $t_j(\lambda)$, only the reflectance $R_j(\lambda)$ of the material printed with colorant j must be measured. Using the measured reflection spectrum R_w of the unprinted medium, the Lambertian reflection $r_g(\lambda)$ is obtained as follows:

$$r_g(\lambda) = \frac{R_w(\lambda)}{(1 - r_{int})(1 - r_{spec}) + R_w(\lambda) r_{int}}, \tag{A11}$$

and the transmission of the certain colorants can be calculated using the following equation:

$$t_j(\lambda) = \sqrt{\frac{R_j(\lambda) - r_{spec}}{r_g(\lambda)[(R_j(\lambda) r_{int} + (1 - r_{int})(1 - r_{spec})]}}. \tag{A12}$$

APPENDIX B: EXAMPLE OF INPUT PARAMETERS FOR THE SIMULATION

Figure 19(a) shows the Lambertian reflectance $r_g(\lambda)$ calculated using Eq. (A11) and, exemplarily for the colorants cyan, magenta, and yellow, the transmission calculated using Eq. (A12). Figure 19(b) shows the relative transmissions $T_c(\lambda)$, $T_m(\lambda)$, and $T_y(\lambda)$ of the three colors cyan, magenta and yellow calculated using Eq. (7) for the

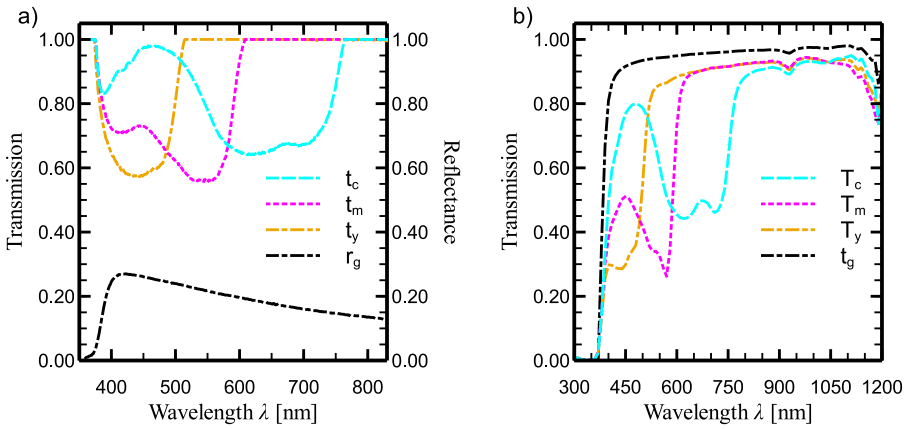

FIG. 19. (a) Lambertian reflectance $r_g(\lambda)$ and calculated transmission through the cyan $t_c(\lambda)$, magenta $t_m(\lambda)$, and yellow $t_y(\lambda)$ colorants. (b) Relative transmissions $T_c(\lambda)$, $T_m(\lambda)$, and $T_y(\lambda)$ of the samples printed with cyan, magenta, and yellow and the internal transmission $t_g(\lambda)$.

simulation of EQE and the internal transmission $t_g(\lambda)$ determined using Eq. (8).

DATA AVAILABILITY

The data that support the findings of this study are openly available in the Research Data Repository of the Leibniz Universität Hannover at https://doi.org/10.25835/0056607.[22]

REFERENCES

[1]G. Eder, G. Peharz, R. Trattnig, P. Bonomo, E. Saretta, F. Frontini, C. S. Polo López, H. R. Wilson, J. Eisenlohr, N. M. Chivelet *et al.*, "Coloured BIPV: Market, research and development," IEA PVPS Task 15, Report IEA-PVPS T15-07 (2019).
[2]G. Peharz and A. Ulm, "Quantifying the influence of colors on the performance of c-Si photovoltaic devices," Renewable Energy **129**, 299–308 (2018).
[3]J. Halme and P. Mäkinen, "Theoretical efficiency limits of ideal coloured opaque photovoltaics," Energy Environ. Sci. **12**, 1274–1285 (2019).
[4]T. Gewohn, M. R. Vogt, B. Lim, C. Schinke, and R. Brendel, "Postproduction coloring of photovoltaic modules with imprinted textiles," IEEE J. Photovoltaics **11**, 138–143 (2020).
[5]J. Schanda, *Colorimetry: Understanding the CIE System* (John Wiley & Sons, 2007).
[6]ICIE, *Improvement to Industrial Colour-Difference Evaluation* (Commission Internationale de l'Éclairage Vienna , 2001).
[7]Z. Schuessler, Defining delta E, https://zschuessler.github.io/DeltaE/learn/; accessed 8 February 2021.
[8]H. R. Kang, *Digital Color Halftoning* (SPIE Press, 1999).
[9]J. A. Yule, *Principles of Color Reproduction* (John Wiley & Sons, New York, 1967).
[10]F. R. Clapper and J. A. C. Yule, "The effect of multiple internal reflections on the densities of half-tone prints on paper," J. Opt. Soc. Am. **43**, 600–603 (1953).
[11]E. Demichel, "Le procédé," Soc. Fr. Photogr. **26**, 17–21 (1924).
[12]R. D. Hersch and M. Hébert, "Base models for color halftone reproduction," in *Handbook of Digital Imaging* (John Wiley & Sons, Ltd., 2015), pp. 1–54.
[13]A. Gershun, "Fresnel reflection of diffusely incident light," J. Opt. Soc. Am. **35**, 162–163 (1945).
[14]T. Gewohn, S. Blankemeyer, M. R. Vogt, H. Schulte-Huxel, M. Köntges, B. Lim, C. Schinke, and R. Brendel, "Laminated textiles enabling custom appearance of building integrated photovoltaic modules," in *International Conference EUPVSEC for Photovoltaic Research* (WIP GmbH & Co Planungs-KG, Brussels, Belgium, 2018), pp. 1842–1844.
[15]T. Söderström, P. Papet, and J. Ufheil, "Smart wire connection technology," in *28th European Photovoltaic Solar Energy Conference* (WIP GmbH & Co Planungs-KG , 2013), pp. 495–499.
[16]Freudenberg Performance Materials SE & Co. KG, Light diffuser from freudenberg, 2019.
[17]M. Köntges, H. Schulte-Huxel, S. Blankemeyer, M. R. Vogt, H. Holst, and R. Reineke-Koch, "Measuring the light recovery factor of backsheets in photovoltaic modules," Sol. Energy Mater. Sol. Cells **186**, 175–183 (2018).
[18]International Electrotechnical Commission, International Standard IEC 60904-8, IEC, Geneva, Switzerland, 2014.
[19]M. R. Luo, G. Cui, and B. Rigg, "The development of the CIE 2000 colour-difference formula: CIEDE2000," Color Res. Appl. **26**, 340–350 (2001).
[20]S. M. Sze, *Physics of Semiconductor Devices*, 2nd ed. (Wiley, New York, 1981).
[21]International Electrotechnical Commission, International Standard IEC 60904-9:2007, IEC, Geneva, Switzerland, 2007.
[22]T. Gewohn, M. R. Vogt, B. Lim, C. Schinke, and R. Brendel (2021). "Dataset: Reflectance and EQE measurements of CoTex (colored textiles) photovoltaic modules," Research Data Repository of the Leibniz Universität Hannover. https://doi.org/10.25835/0056607.